University of Bath

Aligned macroporous TiO_2/chitosan/reduced graphene oxide (rGO) composites for photocatalytic applications

Chao Chen[1], Yan Zhang[2, *], Jing Zeng[1], Fuqiang Zhang[1], Kechao Zhou[1],

Chris R. Bowen[2], Dou Zhang[1, *]

[1]State Key Laboratory of Powder Metallurgy, Central South University, 410083, China

[2]Department of Mechanical Engineering, University of Bath, BA2 7AY, United Kingdom

Abstract: In this paper ice templating is used to fabricate novel TiO_2/chitosan/reduced graphene oxide (rGO) composites with a highly aligned macroporous structure for photocatalytic applications. The structure of the composites was readily tailored using the composite composition, for example the lamellar pore width decreased from 50-45 μm to 5-10 μm, while the lamellar thickness increased from 2-3 to 20-25 μm, with an increase of the TiO_2 content from 45 to 77 vol.%. Lamellar pore channels between the layers exhibited a more uniform distribution when the rGO content was 1.0 wt.%. The increase in viscosity of the composites with high TiO_2 contents led to the formation of smaller ice crystals and smaller lamellar pore sizes to enable the production of composite structures with improved mechanical strength. The TiO_2/chitosan/rGO composites exhibited excellent photocatalytic degradation of methyl orange and the photocatalytic efficiency was optimized by control of the active material content and microstructure. The hybrid composites with 1.0 wt.% rGO showed a degradation percentage of 97%, which makes these novel TiO_2/chitosan/rGO freeze cast structures attractive materials as high performance and high strength substrates for photocatalytic degradation applications.

Keywords: photocatalytic, aligned porous, composite, reduced graphene oxide

---

* Corresponding authors: y.zhang2@bath.ac.uk, dzhang@csu.edu.cn

1. Introduction

The use of photo-degradation to remove organic pollutants has attracted attention as an alternative approach in solving environmental problems and pollution control, as compared to other physical, chemical, and biological technologies [1, 2]. Among the many candidate materials systems for photo-catalysis, TiO_2 has been the most promising candidate due to its good physical and chemical stability, low cost, superior photocatalytic performance and environmental friendliness [3, 4]. However, due to the wide band gap of this material (3.2 eV), it will only absorb a narrow range of the solar spectrum and this leads to a low photocatalytic efficiency which is a concern for its practical application in photocatalytic decontamination [5].

A variety of approaches have been explored to expand the optical response of TiO_2-based materials to a wider range of the solar spectrum. Examples employed to improve the photocatalytic efficiency of TiO_2 include surface sensitization using dyes or carbon materials [6], doping with metal or non-metal elements [7, 8], depositing noble metals and preparing composite semiconductors [9]. Recently, more attention has been paid to natural polymers, such as chitosan [10]. Chitosan is generally obtained by deacetylation of chitin, and it is attractive as it has excellent properties for adsorption during photocatalytic processes; this is due to the presence of hydroxyl (–OH) and amino groups (–NH$_2$) within its structure [11]. The reactive functional groups in chitosan are able to provide sites for numerous chemical reactions on the surface of TiO_2 if a composite of the two materials is formed. In addition, reduced graphene oxide (rGO) has been reported to provide improved dispersion in water, compared to pure graphene [12], and the residual functional groups are beneficial to achieve a strong bonding between the rGO and other additives, such as TiO_2 and chitosan [13]. The combination of TiO_2 and rGO can not only effectively enhance the interface coupling within the composites, but also facilitate the separation of electron and hole pairs in the photochemical reaction [14]. As a result, the formation for TiO_2/chitosan/rGO provides a promising route to enhance the

photocatalytic activity of TiO_2-based composites.

In addition to these active materials, the formation of porous TiO_2 structures has drawn attention due to the enhanced surface-to-volume ratio and reduced diffusion path length to allow a robust interaction of the material with any solvent [15-17]. Recently, porous TiO_2 has been shown to exhibit a much higher photocatalytic activity compared to dense/solid materials due to their stronger adsorption to substrates and/or higher light-harvesting ability [18, 19]. The void space can lower the density, increase the active area for catalysis and improve the ability of the catalyst to withstand cyclical changes in volume. One approach to manufacture porous materials is to use 'freeze casting', also called 'ice templating' which can be readily used to create hierarchical microstructures using a wide range of materials, such as ceramics, metals, polymers and composites [20-22].

In this paper, a facile and environmentally friendly approach is utilized for the synthesis of porous TiO_2/chitosan/reduced graphene oxide composites for photocatalytic decontamination via a one-step freeze casting process. In order to provide detailed information and find the most useful combination of the materials, structure and properties for photo-degradation applications, the morphology, and pore structure of a range of composite compositions were investigated in detail to enhance the photocatalytic efficiency and mechanical properties of the composites. This work provides environmentally friendly and low energy consumption approach to fabricate TiO_2-based composites as photo-catalysts with high efficiency and activity in environment remediation and repeated photocatalytic use.

2. Material and methods

2.1 Preparation of reduced graphene oxide (rGO)

Graphene oxide (GO) was synthesized from natural graphite powder by a modification of Hummers method [23]. In brief, 2 g of graphite, 2 g of $NaNO_3$, and 92 ml of concentrated

H$_2$SO$_4$ were stirred together in an ice bath. Then, 12 g of KMnO$_4$ was slowly added into the bath. The solution was then stirred at 35 °C for 1 h. Deionized water with a volume of 160 ml was added and the temperature was maintained at 90 °C for 30 min. Finally, 400 ml of pure water and 12 ml of H$_2$O$_2$ (30%) was added into the mixture. The solution was filtered and the filter cake was dispersed in water by an ultrasonic bath. The mixture was washed with a 1:10 HCl solution and deionized water by repeated centrifugation. The obtained sediment was dispersed in water with the help of an ultrasonic bath and dried in air at 45 °C overnight. To obtain the rGO, 0.3 g of GO was dispersed in 500 mL deionized water and mixed with 20 mL of N$_2$H$_4$·H$_2$O$_4$ solution for 12 h at 95°C. The mixture was then filtered and washed using ethanol and deionized water for several times. The obtained rGO sediments were dried at 60 °C for 24 h.

2.2 Treatment of the TiO$_2$ powder

Figure 1 shows a transmission electron microscopy (TEM) image of the commercial TiO$_2$ (Sinopharm Chemical Reagent Co, Ltd (SCRC)) powders used for preparing the aqueous dispersions for this work. The powder was composed of particles with an average diameter 90-100nm. For preparing dispersions, 2 g of TiO$_2$ powder was dissolved in 40 mL of distilled water, then the resulting solution were dispersed by means of a tumbling ball mill at 15 r/min for 24 h. The TiO$_2$ dispersions exhibited excellent time stability (over 8 h), which represented a suitable time for preparing and processing composites, with neither sedimentation nor precipitation occurring during this period.
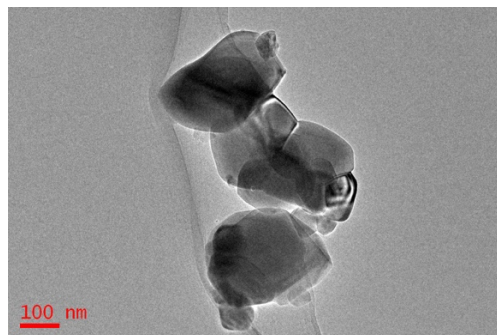

Figure 1 TEM image of the commercial TiO$_2$ powder.

2.3 Preparation of macroporous cross-linked TiO_2/chitosan/rGO composites

All chemicals were of analytical grade and were used without further purification to create the composites. First, chitosan was dissolved in a 2 wt% acetic acid aqueous solution to form a chitosan solution of 2.5 wt%. The solution was then stirred at room temperature for 24 h, filtered, and then placed in an ultrasonic bath for 20 min. Then, 20 mL of the acidified chitosan solution was cross-linked by mixing with 1 mL of γ-glycidoxypropyltrimethoxysilane (GPTMS, Gelest-ABCR), which was used for the fabrication of the porous composites. A volume of 4 mL of an as-prepared chitosan gel cross-linked with GPTMS was mixed with 4 mL of the TiO_2 suspension (50 mg/mL), followed by adding rGO into the mixed suspension and stirred at room temperature for 24h.

In this research, different additions of rGO and TiO_2 based on the water solvent were utilised to create a range of composite compositions and structures, which were 0, 0.5, 1.0, and 1.5 wt.% of rGO and the TiO_2 contents of 45, 62, 71, and 77 vol.%, respectively. The volume ratio of cross-linked chitosan solution to aqueous TiO_2 suspension was controlled to be 1:1, 1:2, 1:3, and 1:4, designated as T45/CS55, T62/CS38, T71/CS29, and T77/CS23, respectively, with the TiO_2 content ranging from 45-77 vol.%. Freeze casting of the above suspensions were carried out by pouring the suspension into a transparent cylindrical polydimethylsiloxane mold, which were then transported to a copper double-side cooling setup which was cooled from room temperature to liquid nitrogen temperature, as shown in Fig. 2. Frozen samples were then demolded and then placed into the vacuum chamber (<10 Pa) of a freeze-drier (FD-1A-50, Beijing Boyikang Medical Equipment Co., China) for 24 h to allow the ice to sublimate.
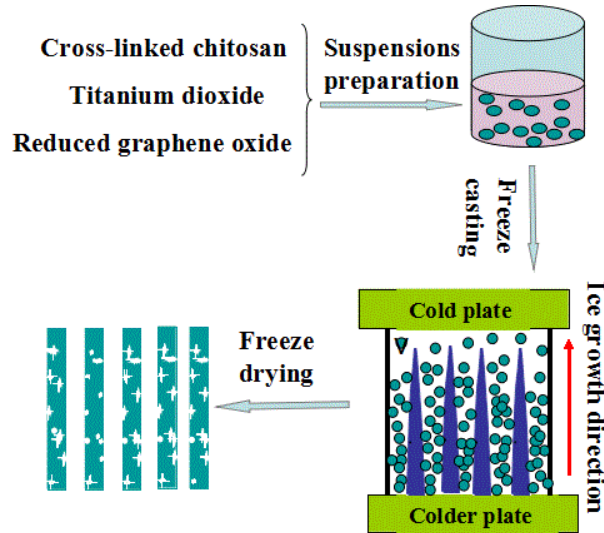
Figure 2. Schematic illustration of the preparation procedures for porous TiO_2/chitosan/rGO composites.

2.4 Characterization of composite materials

Field emission scanning electron microscopy (SEM, NOVA NANOSEM 230) was used to examine the composite microstructure. To evaluate the mechanical properties, uniaxial compression testing were performed on samples of ~9 mm diameter and ~7 mm height at a crosshead speed of 0.2 mm/min using an electronic universal testing machine (KD11-2, Shenzhen KEJALI Technology Co. Ltd., China). A minimum of five independent stress-strain measurements were obtained per sample. Transmission electron microscopy (TEM) images were obtained from a JEOL JEM–2100 operated at an accelerating voltage at 200 kV. The crystal structure of the samples was examined in θ–2θ mode by X-ray diffraction (XRD, Rigaku D–Max/2550VB$^+$) utilizing Cu K_α radiation (λ=1.5418 Å). Fourier-transform infrared (FT-IR) spectroscopy was performed with a Nicolet 6700 instrument over the range of 4000–450 cm^{-1} to determine functional groups of the samples.

2.5 Photocatalytic activity of TiO_2/chitosan/rGO hybrid composites

The photocatalytic activity of the TiO_2/chitosan/rGO composites was evaluated by

investigating decolorization of methyl orange solutions at room temperature. For this process, TiO$_2$/chitosan/rGO composites were cut into cylindrical pieces (diameter of 5mm, length of 10 mm) and placed in a Petri dish containing 100 mL of methyl orange solution (250 mg/L). In each experiment, the Petri dish was kept in the dark for 1 h prior to UV light illumination to achieve adsorption and desorption equilibria. Subsequently, solutions were irradiated using a UV lamp (λ=365 nm), and at given irradiation time intervals (every 30 min), 2 mL of the sample were then collected and the residual concentration of dye molecules measured by monitoring the change in absorbance at 464 nm for methyl orange, respectively. Calibration graphs for each dye were used to determine time dependent changes in dye concentration in the irradiated solutions. Control experiments in the absence of light or chitosan scaffolds prepared without graphene were also performed.

3. Results and discussion

In this study, rGO was synthesized from graphite powder by a Hummers method. As shown in Fig. 3(a), the XRD spectra of the parent graphite GO and rGO show the transformation of the interlayer spacing, which is a clear indication of a complete transformation from graphite to rGO. The parent graphite has a sharp peak at 26.4°, which was from the diffraction of the (002) planes of graphite. After oxidation, the peak at 26.4° disappeared and a peak at 10.9° was detected, indicating the transition from graphite to GO. A broad peak near 24° revealed the production of rGO after reduction of GO by N$_2$H$_4$·H$_2$O$_4$. FT-IR experiments were also carried out to investigate the transformation from graphite to rGO. As shown in Fig. 3(b), in the spectrum of GO, the peak at 1724 cm^{-1} is a characteristic of the C=O stretch of the carboxylic group on the graphene oxide. The absorption band appearing near 1600 cm^{-1} in the spectrum of rGO clearly showed the skeletal vibration of the graphene sheets, indicating the formation of rGO during the hydrothermal reaction. The above results further confirmed the

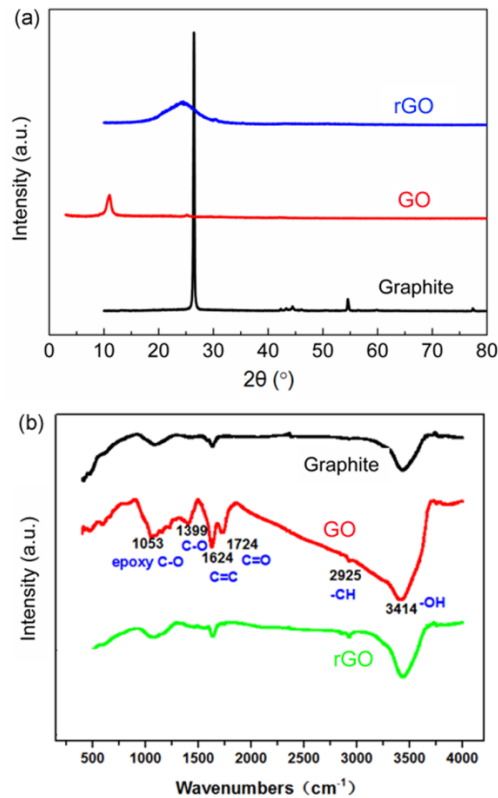transformation from graphite to rGO.

Fig 3 (a) XRD and (b) FT-IR diagrams of graphite, GO and rGO.

Fig. 4 (a-d) shows scanning electron microscopy (SEM) micrographs of the porous TiO_2/chitosan/rGO composites with 1.0 wt.% rGO and a TiO_2 content of 45, 62, 71, and 77 vol.%, respectively. With an increase of the TiO_2 content, the lamellar pore width decreased from 50-45 μm to 5-10 μm, while the lamellar thickness increased from 2-3 μm to 20-25 μm. In Fig. 4 (a-c), the detailed dendritic characteristics of the freeze cast structures can be observed on the surface of the lamellar wall as the TiO_2content increased from 45 vol.%to 71 vol.%. However, the lamellar surface became smooth when the TiO_2 content increased to 77 vol.%. According to our previous studies [24, 26], as the solid loading of the suspension increases, the viscosity also increases, resulting in a large resistance to the rearrangement of particles to form a replica of the ice structures during the unidirectional solidification process, as shown in Fig. 2. This increased viscosity

therefore leads to the formation of smaller ice crystals and therefore smaller lamellar pore sizes are obtained. Consequently, the fabrication of lamellar porous structures with a smaller pore size can be achieved by increasing the solid loading of the suspension and this enables the formation of composite structures with improved mechanical strength that are easy to be handled more easily during the fabrication process and are more robust to the working conditions of the materials.
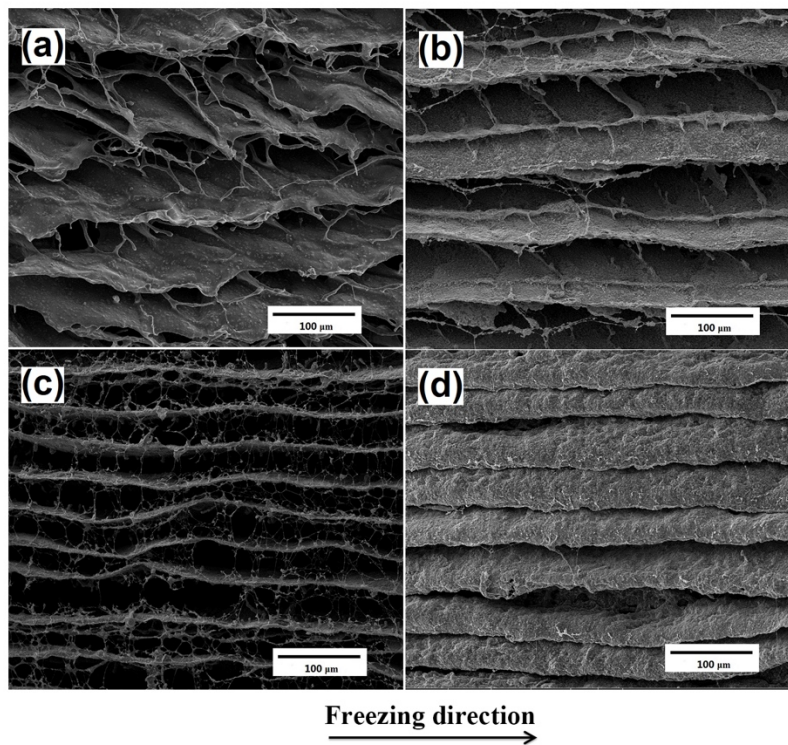

Freezing direction

Figure 4 SEM images of porous TiO_2/chitosan/rGO composites prepared by 1.0 wt.% rGO with TiO_2 contents of (a) 45 vol.%, (b) 62 vol.%, (c) 71 vol.%, and (d) 77 vol.%.

Fig. 5 (a-d) shows the SEM micrographs of porous TiO_2/chitosan/rGO composites with 45 vol.% TiO_2 and rGO contents ranging from 0, 0.5, 1.0 and 1.5 wt.%, respectively. The pore channels exhibited an aligned network along the freezing condition, which can be observed at all ranges of rGO contents, as in our previous studies [24, 25]. With an increase of the rGO content, the lamellar pore structures became more distinct. When the rGO content reached 1.0 wt%, as in Fig. 5(c), the channels between the layers are clearly

visible and exhibit a uniform distribution with a lamellar pore width of 40 to 50 μm and a lamellar wall thickness of 2 to 3 μm. During the directional freezing casting process, the rGO, chitosan chains and the TiO$_2$ nanoparticles are rejected and entrapped by the adjacent ice crystals, resulting in the formation of a macro-porous structure. The highly aligned lamellar pore structure is advantageous for photocatalytic applications as it provides an easy pathway for mass transfer and minimizes the pressure drop inside the monoliths, which facilitates effective photocatalytic reactions in decontamination. However, the uniformity of the lamellar pore structures begins to disappear when the rGO content is increased to 1.5 wt%, as shown in Fig. 5(d). The parallel nature of the lamellar pore channel decreased with large additions of rGO and maybe related to the less uniform distribution of the rGO when the amount of rGO in the composite mixture exceeds 1.5 wt.%.
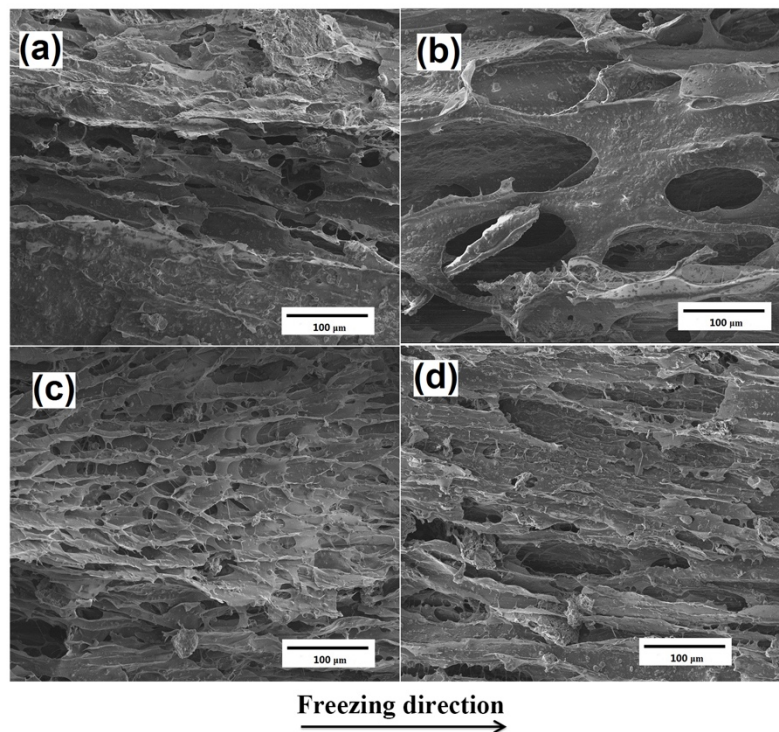

Figure 5 SEM images of porous TiO$_2$/chitosan/rGO composites prepared by 45 vol.% TiO$_2$ with rGO contents of (a) 0, (b) 0.5 wt.%, (c) 1.0 wt.%, and (d) 1.5 wt.%.

Fig. 6 (a) and (b) show the compressive stress-strain curves of porous TiO_2/chitosan/rGO composites with TiO_2 contents ranging from 45 vol.% to 77 vol.% and rGO contents ranging from none to 1.5 wt.%, respectively. The compressive load was applied parallel to the freezing direction, as shown in Fig. 4 and 5, as in our previous work [26]. All the stress-strain curves in Fig. 6 exhibited almost linear elasticity for stress levels up to a yield point, followed by a collapse of the stress after a plateau, which probably resulted from buckling of the ceramic wall structure under compression. As a result of the thick ceramic walls formed by the high solid loading, an in accordance to our previous results [26], the compressive strength increased from 0.09 MPa to 0.14 MPa with an increase of the TiO_2 content, as shown in Fig. 6 (a). However, the compressive strength of the porous TiO_2/chitosan/rGO increased and reached a maximum value of 0.11 MPa at an rGO content of 0.5 wt.%, followed by the decrease in the compressive strength with a further increase of the rGO content from 1.0 to 1.5 wt.%. This level of strength is almost twice as high as TiO_2/chitosan composites formed the same freeze casting method [27], indicating that rGO and the more aligned pore channels had a beneficial effect on improving the mechanical properties of chitosan composite scaffolds.
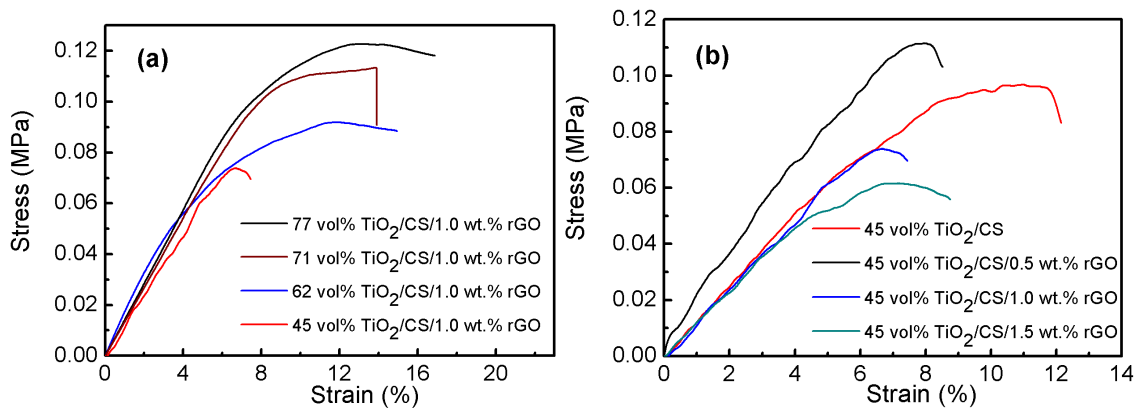

Figure 6 Compressive stress–strain curves of porous TiO_2/chitosan/rGO scaffolds with (a) 1.0 wt% rGO and different additions of TiO_2 ranging from 45 to 77 vol.% and (b)45 vol.% of TiO_2 and different amounts of rGO ranging from 0 to 1.5 wt.%.

The potential photocatalytic application of the as-prepared porousTiO$_2$/chitosan/rGO composites was evaluated by testing scaffold sections for their activity in terms of oxidative degradation of methyl orange. When incubated in methyl orange solutions, the TiO$_2$/chitosan/rGO scaffolds turned orange in color, indicating strong adsorption of the dye molecules. Subsequent irradiation with UV light resulted in decolorization of the methyl orange-loaded TiO$_2$/chitosan/rGO composite scaffolds, confirming that the scaffold sections exhibited substantial photocatalytic activity. The faster rate of photo degradation of the methyl orange molecules was attributed to increased adsorption of the anionic dye on the surface of the positively charged TiO$_2$ matrix compared with surface binding of cationic methyl orange. In contrast, no decolorization of the dye solutions was observed for cross-linked chitosan/rGO prepared in the absence of TiO$_2$ particles. A time dependent concentration plot is shown in Fig. 7, it can be seen that the photocatalytic activity of the TiO$_2$/chitosan/rGO composites can be improved by the addition of TiO$_2$. The rate of methyl orange degradation for composites with 62 vol.% of TiO$_2$ was significantly higher than that with lower amounts of 45 vol.% TiO$_2$. This was attributed not only to the increased TiO$_2$ content but also due to the lamellar porous structure of the composite which exhibited a small pore size and dendritic characteristic on the surface of the lamellar wall, as in Fig. 5(c). It is noted that the samples with 62 vol.% and 71 vol.% of TiO$_2$, compared to the samples with lower amounts of TiO$_2$, exhibited a low efficiency ratio of the photocatalytic reaction at the initial stages of degradation process (0~40 min in Fig. 7), although these samples then exhibited a higher rate of degradation of methyl orange at later stages of the process. Since the sample with 45 vol.% TiO$_2$ has a large but irregular pore structure (Fig. 5(a)), the methyl orange could initially react with TiO$_2$ quickly at the surface of the scaffold. However, the disordered pore structure restricted a further increase of the degree of degradation of methyl orange. Fig. 7 shows that a further increase of the TiO$_2$ content above 71 vol.% led to the deterioration of the effects of decolorization of the TiO$_2$/chitosan/rGO composites. Samples with 77 vol.% TiO$_2$

exhibited a low rate of degradation, compared to 62 vol.% and 71 vol.%, as a result of the lamellar surface becoming smooth (as shown in Fig. 4d), with a correspondingly smaller <mark>surface area</mark>.
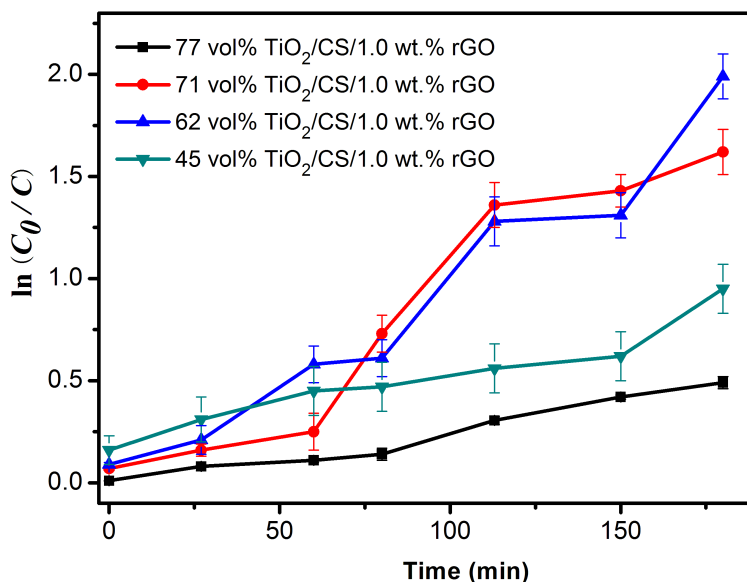

Figure 7 Photocatalytic degradation plots showing decolorization for methyl orange adsorbed onto macroporous TiO_2/chitosan/graphene composites with different additions of TiO_2.

Fig.8 shows the photocatalytic degradation ratio of TiO_2/chitosan/graphene composites under UV illumination. As shown in Fig. 8(b), with the addition of 0.5 wt.% rGO the degradation percentage of the TiO_2/chitosan/graphene composite reached 90.4%, compared to 74.6% for the TiO_2/chitosan scaffold without rGO. When the rGO content increased to 1.0 wt.%, the degradation percentage increased further and reached a maximum of 97%. The rGO sheets in the composite act to increase the photo-absorption and scattering which leads to an increase of the photocatalytic activity of the composites. The TiO_2/chitosan/graphene composites with 1.0 wt.% of rGO also show a uniform distribution of lamellar pore structures, as shown in Fig. 4(c). The highly aligned lamellar pore structure provides an easy path for the molecular transfer and minimizes the

pressure drop inside the monoliths [27, 28], which facilitates effective photocatalytic degradation of methyl orange. However, the degradation rate decreased to 87.8% when the rGO content increased to 1.5 wt.%, due to the rGO in to the matrix lowering the contact surface area of TiO_2 with methyl orange, as shown in Fig. 5(d).
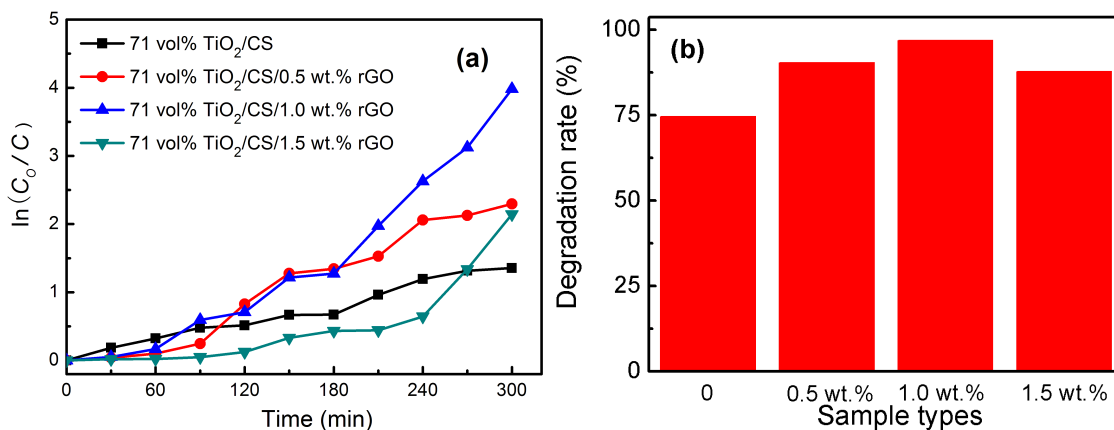

Figure 8 (a) Photocatalytic degradation plots showing decolorization for methyl orange adsorbed onto macroporous TiO_2/chitosan/graphene composites with different additions of rGO. (b) Histogram of degradation rate after 300 min.

4. Conclusions

In this study, highly oriented macro-porous TiO_2/chitosan/ reduced graphene oxide (rGO) composites for photocatalytic applications were fabricated using water-based freeze casting. The highly aligned porous composites exhibited distinct lamellar structures with a pore width of 40 to 50 μm and a lamellar wall thickness of 2 to 3 μm. The addition of rGO and the resulting aligned pore channels were beneficial in improving the mechanical properties of chitosan scaffolds. The aligned lamellar pore structure was also advantageous for photocatalytic applications since it provides an easy pathway for mass transfer inside the monoliths, which facilitates effective photocatalytic reactions in decontamination. The amount of TiO_2 was tuned to improve the photocatalytic activity of

the TiO_2/chitosan/rGO composites and the rate of methyl orange degradation for the samples with 71vol.% of TiO_2 was significantly higher than other systems by control of the active material content and composite architecture. A degradation percentage of 97% was obtained in the samples with 1.0 wt.% of rGO, while using rGO contents above 1.0 wt.% lead to decreased photocatalytic activity due to a reduction of the surface area of the composite materials. These novel TiO_2/chitosan/rGO structures are attractive materials as high performance, low-cost and high strength materials for photocatalytic degradation applications.

References

[1] E. V. Kondratenko, G. Mul, J. Baltrusaitis, G. O. Larrazábal, J. Pérez-Ramírez, Status and perspectives of CO_2 conversion into fuels and chemicals by catalytic, photocatalytic and electrocatalytic processes. Energ. Environ. Sci. 6 (2016) 3112-3135.

[2] S. C. Roy, O. K. Varghese, M. Paulose, C. A. Grimes, Towardsolarfuels: Photocatalytic conversion of carbon dioxide to hydrocarbons. ACS Nano. 4 (2010) 1259-1278.

[3] K. Babu, M. Duraiselvam. Surface nano-texturing of silicon by picosecond laser irradiation through TiO$_2$ nanotube arrays. Appl. Surf. Sci. 353 (2015) 1112-1116.

[4] L. Sun, Z. L. Zhao, Y. C. Zhou, L. Liu. Anatase TiO$_2$ nanocrystals with exposed {001} facets on grapheme sheets via molecular grafting for enhanced photocatalytic activity. Nanoscale, 4 (2012) 613-620.

[5] Y. Cong, X. Li, Y. Qin, Z. Dong, G. Yuan, Z. Cui, X. Lai. Carbon-doped TiO$_2$coating on multiwalled carbon nanotubes with higher visible light photocatalytic activity. Appl. Catal. B: Environ. 107 (2011) 128-134.

[6] C. Andriantsiferana, E. F. Mohamed, H. Delmas. Photocatalytic degradation of an azo-dye on TiO$_2$/activated carbon composite material. Environ. Technol. 35 (2014) 355-363.

[7] B. Liu, H. Chen, C. Liu, S. Andrews, C. Hahn, and P. Yang. Large-Scale Synthesis of Transition-Metal-Doped TiO$_2$ Nanowires with controllable over potential. J Amer. Chem. Soc. 135 (2013) 9995-9998.

[8] J. Xu, Y. Ao, M. Chena and D. Fu. Photoelectro chemical property and photocatalytic activity of N-doped TiO$_2$ nanotube arrays. Appl. Surf. Sci. 256 (2010) 4397-4401.

[9] L. Gomathi Devi, R. Kavitha. A review on plasmonic metal-TiO$_2$ composite for generation, trapping, storing and dynamic vectorial transfer of photogenerated electrons across the Schottky junction in a photocatalytic system. Appl. Surf. Sci. 360 (2016) 601-622.

[10] Y. Haldorai, Jae-Jin Shim. Novel chitosan-TiO$_2$ nanohybrid: Preparation, characterization, antibacterial, and photocatalytic properties. Polym. Composite. 35 (2014) 327-333.

[11] N. Acosta, C. Jimenez, V. Borau, A. Heras. Extraction and characterization of chitin from crustaceans. Biomass Bioenergy, 5 (1993) 145-153.

[12] D. Konios, M. M. Stylianakis, E. Stratakis, E. Kymakis. Dispersion behaviour of graphene oxide and reduced graphene oxide. J Colloid Interf. Sci. 430 (2014) 108-112.

[13] D. Chanda, J. Hnát, A. S. Dobrota, I. A. Pašti, M. Paidar and K. Bouzek. The effect of surface modification by reduced graphene oxide on the electrocatalytic activity of nickel towards the hydrogen evolution reaction. Phys. Chem. Chem. Phys. 17 (2015) 26864-26874.

[14] G. Nagaraju, G. Ebeling, R. V. Gonçalves, S. R. Teixeira, D. E. Weibeld, J. Dupont. Controlled growth of TiO_2 and TiO_2-RGO composite nanoparticles in ionic liquids for enhanced photocatalytic H_2 generation. J. Mol Catal A-Chem. 378 (2013) 213-220.

[15] S. Yang, C. Cao, P. Huang, L. Peng, Y. Sun, F. Wei and W. Song. Sandwich-like porous TiO_2/reduced graphene oxide (rGO) for high-performance lithium-ion batteries. J. Mater. Chem. A 3 (2015) 8701-8705.

[16] A. Tricoli, A. S. Waller and M. Righettoni. Highly porous TiO_2 films for dye sensitized solar cells. J. Mater. Chem. A 22 (2012) 14254-14261.

[17] J. Fei, J. Li. Controlled preparation of porous TiO_2-Ag nanostructures through supramolecular assembly for plasmon-enhanced photocatalysis. Adv. Mater. 2(2015) 314-319.

[18] K. Lv, J. Yu, J. Fana and M. Jaroniec. Rugby-like anatasetitania hollow nanoparticles with enhanced photocatalytic activity. Cryst. Eng. Comm. 13 (2011) 7044-7048.

[19] X. Lou, L. A. Archer. A general route to nonspherical anatase TiO_2 hollow colloids and magnetic multifunctional particles. Adv. Mater. 20 (2008) 1853-1858.

[20] S. Yook, H. Jung, C. Park, K. Shin, Y. Koh, Y. Estrin, H. Kim. Reverse freeze casting: A new method for fabricating highly porous titanium scaffolds with aligned large pores. Acta Biomater. 8 (2012) 2401-2410.

[21] Y. Zhang, L. Chen, J. Zeng, K. Zhou, D. Zhang. Aligned porous barium titanate/hydroxyapatite composites with high piezoelectric coefficients for bone tissue engineering. Mater. Sci. Eng. C. 39 (2014) 143-149.

[22] K. Yang, Z. Li. Synthesis and Characterization of PVA/MMT porous nanocomposite Prepared by directional freeze-drying method. Adv. Mater. Res. 197-198 (2011) 253-260.

[23] W. S. Hummers, R.E. Offeman. Preparation of graphitic oxide. J. Am. Chem. Soc. 80 (1958) 1339.

[24] Y. Zhang, K. Zhou, J. Zeng, D. Zhang. Control of pore structures and sizes in freeze cast ceramics. Adv. Appl. Cera. 112 (2013) 405-411.

[25] Y. Zhang, Y. Bao, D. Zhang, C. R. Bowen. Porous PZT ceramics with aligned pore channels for

energy harvesting applications. J. Am. Cera. Soc. 98 (2015) 2980-2983.

[26] Y. Zhang, K. Zhou, Y. Bao, D. Zhang. Effects of rheological properties on ice-templated porous hydroxyapatite ceramics. Mater. Sci. Eng. C. 33 (2013) 340-346.

[27] C. Suwanchawalit, A. J. Patil, R. Kumar, S. Wongnawa and S. Mann. Fabrication of ice-templated macroporous TiO_2-chitosan scaffolds for photocatalytic applications. J. Mater. Chem. 19 (2009) 8478-8483.

[28] B. Liu, L. Chen, C. Shao, F. Zhang, D. Zhang Improved osteoblasts growth on osteomimetic hydroxyapatite/$BaTiO_3$ composites with aligned lamellar porous structure. Materials Science & Engineering C. 61 (2016) 8-14.

Figure caption

Figure 1 TEM image of the commercial TiO_2 powder.

Figure 2 Schematic illustration of the preparation procedures for porous TiO_2/chitosan/rGO composites.

Figure 3 (a) XRD and (b) FT-IR diagrams of graphite, GO and rGO.

Figure 4 SEM images of porous TiO_2/chitosan/rGO composites prepared by 1.0 wt.% rGO with TiO_2 contents of (a) 45 vol.%, (b) 62 vol.%, (c) 71 vol.%, and (d) 77 vol.%.

Figure 5 SEM images of porous TiO_2/chitosan/rGO composites prepared by 45 vol.% TiO_2 with rGO contents of (a) 0, (b) 0.5 wt.%, (c) 1.0 wt.%, and (d) 1.5 wt.%.

Figure 6 Compressive stress–strain curves of porous TiO_2/chitosan/rGO scaffolds with (a) 1.0 wt.% rGO and different additions of TiO_2 ranging from 45 to 77 vol.% and (b)45 vol.% of TiO_2 and different amounts of rGO ranging from 0 to 1.5 wt.%.

Figure 7 Photocatalytic degradation plots showing decolorization for methyl orange adsorbed onto macroporous TiO_2/chitosan/graphene composites with different additions of TiO_2.

Figure 8 (a) Photocatalytic degradation plots showing decolorization for methyl orange adsorbed onto macroporous TiO_2/chitosan/graphene composites with different additions of rGO. (b) Histogram of degradation rate after 300 min.